Design tradeoffs between constant power speed range, uncontrolled generator operation and rated current of IPM motor drives

Design tradeoffs between constant power speed range, uncontrolled generator operation and rated current of IPM motor drives

G. Pellegrino
Member, IEEE
gianmario.pellegrino@polito.it

A. Vagati
Fellow, IEEE
alfredo.vagati@polito.it

P. Guglielmi
Member, IEEE
paolo.guglielmi@polito.it

Politecnico di Torino, Corso Duca degli Abruzzi 24, Torino, 10129 Italy

***Abstract* -- A closed-form approximate formulation is proposed to establish a relationship between the uncontrolled generator operation of IPM motors at high speed and the constant power speed range and drive current capabilities. High saliency IPM motors of the PM-assisted synchronous reluctance type are mainly considered in the analysis, since they are proved to have the most favorable ratio between flux weakening capability and uncontrolled generator voltage. The results of the analysis show the tight relationship between the uncontrolled overvoltage and the constant power speed range of the drive. Moreover, where the uncontrolled voltage is higher, the relationship between the constant power speed range and the motor current amplitude becomes stiffer: for small current variations a large reduction of the speed range can occur. The analysis is validated experimentally on two motors of very different size (500 W and 1 MW).**

Index Terms -- Permanent magnet machines, Variable Speed Drives, Synchronous Motor Drives, Traction Motor Drives, Electric Machine Design Methodology.

LIST OF SYMBOLS

λ	stator flux linkage
λ_m	permanent magnet flux linkage
λ_r	reluctance component of stator flux linkage
λ_{rated}	rated flux linkage
λ_{min}	flux linkage at maximum operating speed
T	motor torque
p	number of pole pairs
i_0	rated current of the drive
i_1	minimum current with flat power profile
i_{ch}	characteristic current of the IPM motor
L_d, L_q	direct and quadrature inductances
ξ	motor saliency
γ	phase of current vector respect to the *d* axis
δ	phase of flux vector respect to the *d* axis
ω_{max}	maximum operating speed
r	constant power speed range
V_{rated}	rated phase voltage
V_{UCG}	phase back-EMF at maximum speed

Subscripts

rated	rated condition of the drive (flux, voltage)
r	referring to the reluctance flux component
MTPA	Maximum Torque per Ampere condition
MTPV	Maximum Torque per Volt condition

I. INTRODUCTION

Interior Permanent Magnet (IPM) motors are attractive in many applications for their flux weakening capability, associated with good torque density and high efficiency [1-2]. With respect to induction motors, IPM motors show a better compactness [3], and a smaller inverter size when a large constant power speed range (CPSR) is required, since the pull-out torque limit [4] can be shifted at theoretically infinite speed with a proper motor design [5]. To achieve the willed CPSR the correct matching of permanent magnet (PM) flux and rotor magnetic saliency must be found [5]. In general, large speed ranges are possible either with non salient rotors with surface mounted PMs and concentrated windings [6], or with multi layer IPM rotors with a high saliency and inset PMs. In particular, the latter ones show a reduced PM flux (with respect to the machine rated flux) that is beneficial in terms of uncontrolled generator (UCG) operation, in case of inverter shutdown at high speed, when the motor back-emf can induce currents back to the dc link [7]. The UCG fault can be lethal for the inverter if the dc voltage rise is not properly limited.

The first goal of the paper is to establish a closed-form relationship between the CPSR capability and the UCG overvoltage of IPM motors. Although this relationship is valid for all IPM motors, in general, the attention will be devoted here to those ones with a high saliency ratio (ξ) and a reduced PM per-unit flux ($\lambda_m/\lambda_{rated}$). Such motors are basically synchronous reluctance (SR) motors where a proper quantity of PMs is added into the rotor core. That is why they are preferably indicated as PM-assisted synchronous reluctance (PMASR) motors [8-10]. As a first conclusion, it will be pointed out that PMASR motors are more suited to applications requiring large CPSRs then PM motors with a

lower saliency or no saliency at all [11].

The second goal of the paper is to evaluate how sensitive the CPSR of an IPM motor is towards a change of the current amplitude. All PM motor drives can have an ideally flat power profile when their current equals the characteristic (short circuit) current of the motor ($i_{ch} = \lambda_m / L_q$), but as soon as the current gets higher or lower than this specific value the power curve at constant current amplitude can drop quite suddenly with speed, depending on the motor design. It is then important to establish how it is possible to obtain a wide current range, centered around the characteristic value, where the power versus speed curve of the drive is still nearly flat. Having such flexibility towards the current amplitude might be important for two reasons. First: the same motor design can be associated to different nameplates, with the current rating referring to the various cooling setups (e.g. natural air or forced ventilation or liquid cooling) and load specifications. Second: a drive with flat power curves at the different current levels is advantageous where the duty time at high speed and reduced power is significant, like in traction. Otherwise, it means an extra current component is needed for flux-weakening, giving additional copper losses. For such very different reasons it is important to establish whether a current that is higher of lower than the rated one still leads to a power curve that is nearly flat or not. It will be shown that machines with a low UCG voltage are more flexible from this point of view, while machines with high UCG voltage may have a high CPSR but in a very limited current range.

The model is validated through experimental data over two PMASR machines of very different size, one designed for home appliance (500 W) and the other one for railway roller tests (1 MW), showing a good agreement with experimental data.

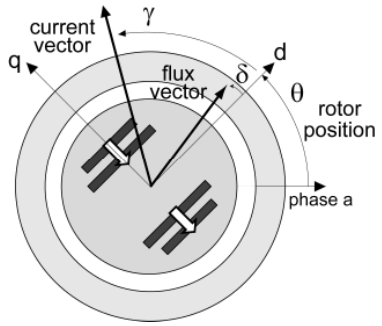

Figure 1. Definition of dq synchronous frame according to PMASR conventions.

II. Constant Power Speed Range and Uncontrolled Generator Voltage

The relationship between CPSR and UCG voltage is investigated, in order to evaluate the required UCG overvoltage for a given CPSR or vice-versa. PMASR motors will be mainly considered, although the results have general validity for all IPM machines.

A. PM-assisted Synchronous Reluctance motor model

PMASR motors have a low per-unit PM flux: $\lambda_m << \lambda_{rated}$, where λ_{rated} is the rated amplitude of the stator flux linkage, corresponding to the maximum torque per Ampere condition at rated drive current i_0. At low speed, when the flux vector and torque are the rated ones, the flux vector happens to be nearly in quadrature with the PM flux and roughly aligned to the direction of maximum permeance, called the *d* axis, as shown both in Figs. 1 and 2. For convenience, the *dq* synchronous frame defined in Fig. 1 has been aligned with the direction of maximum permeance, as usual for SR motors [8] and not with the direction of the magnets, as usual for PM motors.

The considerations in the following are based on the simplified magnetic model (1)-(2), where the machine linked flux vector (λ) is split into the PM flux vector (subscript *m*) and the reluctance flux vector (subscript *r*), that is the one of the basic SR machine, before the PMs are inserted into the rotor.

$$\bar{\lambda} = \bar{\lambda}_m + \bar{\lambda}_r \tag{1}$$

$$\bar{\lambda}_{r,dq} = L_q \cdot \begin{bmatrix} \xi & 0 \\ 0 & 1 \end{bmatrix} \cdot \bar{i}_{dq} \quad ; \quad \bar{\lambda}_{m,dq} = \begin{bmatrix} 0 \\ -\lambda_m \end{bmatrix} \tag{2}$$

The saliency ratio $\xi = L_d / L_q$ (> 1) has been introduced in (2), and the PM flux is aligned with the negative *q* axis, as defined in Fig. 1. Magnetic saturation and cross saturation are not evidenced in the simplified model (2). Nevertheless, they will be properly taken into consideration in the following by setting case by case different ξ values for the different working points, for taking into account the real-world effects (saturation and cross-saturation), according to the experimental magnetic curves of the investigated motor. In the following ξ_{MTPA}, ξ_{MTPV} will be adopted, referring to Maximum Torque per Ampere operation and Maximum Torque per Volt operation respectively. Detailed remarks are given in section IV.

B. Definition of constant power speed range (CPSR)

In the example vector diagram reported in Fig. 2 the PM and reluctance flux components defined in (1) are evidenced at the drive rated current i_0. This corresponds to the inverter current rating and is the current that will be referred to for the design of the PM flux linkage, as explained in the following. It is not necessarily the current corresponding to the continuous power of the motor which is lower than i_0 in most cases. The so defined rated vector situation is represented in Fig. 2 that gives the rated torque from zero to base speed. Base speed is the one at which the inverter voltage limit is reached. The dashed elliptical trajectories represent the flux paths when the current vector is rotated for flux weakening over the base speed. The flux weakening capability of the drive is related to the matching between the characteristic

current of the motor $i_{ch} = \lambda_m / L_q$ and the drive current amplitude i_0. When the available current is close to i_{ch} (larger or smaller) a high CPSR can be obtained, while with current values that are either much higher or much lower than i_{ch} the CPSR tends to drop or even disappear.

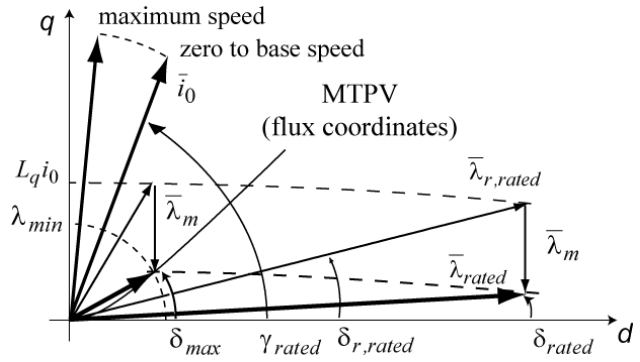

Figure 2. Vector diagram of a PM assisted SR motor at rated drive current (i_0). At low speed, rated torque situation is indicated with "rated". The flux weakening trajectories at constant current amplitude are dashed. At maximum speed (i.e. minimum flux) the flux vector is set exactly on the Maximum Torque per Voltage (MTPV) flux trajectory.

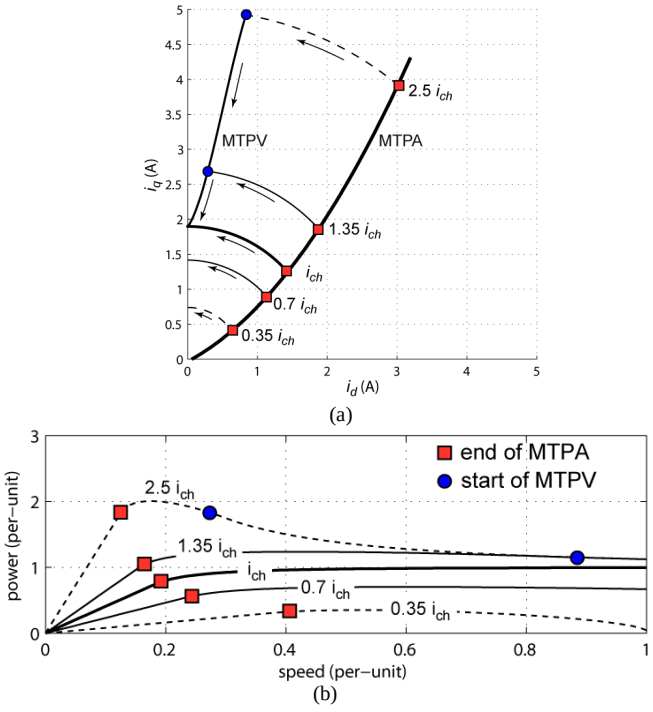

Figure 3. PMASR drive tested at different current amplitudes, centered on the characteristic current value. a) Control trajectories in the *dq* current plane. b) Corresponding power profiles, at limited inverter voltage. The motor is Motor 1, referenced in the Appendix. The *xy* scaling factors are 460 W, 20000 rpm and i_{ch} is 2 A (pk).

In Fig. 3 the flux weakening trajectories at constant current amplitude are reported for a real PMASR drive. Different values of the current amplitude are considered, in a range that spans from well below to well above the characteristic current (0.35 to 2.5 times i_{ch}). Figure 3a reports the current vector trajectories in the *dq* frame, while Fig. 3b reports the corresponding power versus speed curves. The base speed is indicated by a square. Below the base speed the maximum torque per Ampere (MTPA) condition has been assumed for each current. For ***those current values that are larger than*** $\boldsymbol{i_{ch}}$ the maximum torque per voltage (MTPV) region is encountered at a certain speed [5] that has been indicated with a circle in Fig. 3b.

From that speed on, the power curves corresponding to 1.35 i_{ch} and 2.5 i_{ch} drop more or less suddenly depending on how larger is the current with respect to i_{ch}, while they are practically flat within the square to circle speed range. Therefore, if the rated current of the drive i_0 is such that $i_0 > i_{ch}$, the circled speed can be consistently considered as the end of the CPSR region, since the power curve drops from there on, while the squared speed (base speed) is the beginning of the CPSR.

This simplified definition of CPSR at fixed current amplitude will be adopted in the following for its simplicity and tight relation with the vector diagrams used for motor design. It will be also assumed that the drive is designed for having $i_0 > i_{ch.}$ A criterion for expressing the CPSR when the current amplitude is lower than the characteristic one will be also defined, that is for power curves that do not meet the MTPV region, like the ones reported in Fig. 3b (0.35 i_{ch} and 0.7 i_{ch}).

C. Design of the appropriate λ_m

Following the design procedure presented in [12], the PM flux of a PMASR motor is designed for maximizing the motor torque at the target maximum speed and rated drive current i_0 and it is *based on the assumption that the rated current is higher than the characteristic current* ***($i_0 > i_{ch}$)***. At that aim, starting from the characteristics of a preliminarily designed SR motor, the target PM flux is set such that the resulting IPM drive will reach the MTPV region exactly at the maximum operating speed, with the rated current amplitude i_0. The wanted PM flux is obtained by inserting proper quantity of PMs in each rotor layer, according to the geometry of the existing rotor and the adopted PM grade, as addressed in detail in [10]. Once the proper λ_m has been obtained, the vector diagram at maximum speed, rated current must be the one of Fig. 4, where $L_q \cdot i_0$ is representative of the characteristics of the basic SR motor (L_q) and of the current load i_0. The λ_{min} circle refers to the maximum speed condition at rated phase voltage (V_{rated}), according to the relation (3), where resistive drops have been neglected:

$$V_{rated} \cong \omega_{max} \cdot \lambda_{min} \tag{3}$$

It is worth to be noticed that the design process requires some iterations for having the condition of Fig. 4 exactly respected, since the MTPV path of the final IPM machine

also depends on λ_m, as it will be shown analytically in the following.

With this design criterion, based on the maximum speed working condition, the torque and power factor at base speed are not directly determined, but come out as a consequence of the choice of λ_m. The torque is the one of the SR motor plus a contribution that depends on how large the PM flux is, in per-unit of the rated machine flux. The power at base speed might be lower than that at maximum speed, due to a lower power factor, because of the need of magnetizing current, as it will be shown with practical examples in the experimental section. The base speed follows from the high speed design according to the motor saliency, as shown in the following.

D. Uncontrolled generator operation (UCG)

It is useful to define the k_{UCG} factor (4):

$$k_{UCG} = \frac{\lambda_m}{\lambda_{min}} = \frac{\omega_{max} \cdot \lambda_m}{\omega_{max} \cdot \lambda_{min}} \cong \frac{V_{UCG}}{V_{rated}} \tag{4}$$

where V_{UCG} is the motor back-emf at maximum speed. For motors with a significant saliency ($\xi > 2$) an overshoot factor should be also taken into account, for evaluating the peak UCG voltage amplitude correctly, because of the hysteretic behavior described in [7]. However, the general conclusions of this analysis are not affected from this behavior and it will be disregarded here.

Once the PM flux has been determined according to the maximum speed condition as just described, the UCG back-emf at maximum speed follows from (4). In the example of Fig. 4 the overvoltage factor is $k_{UCG} = 1$. The λ_m design procedure introduced in subsection II.C will be now expressed analytically and the approximate relationship (18) between the UCG overvoltage factor k_{UCG} and the CPSR will be formulated.

E. MTPV trajectory in the dq flux plane [12]

First of all, the expression of electromagnetic torque is recalled (5), showing both the flux and current vectors:

$$T = \tfrac{3}{2}\, p \cdot \bar{\lambda} \times \bar{i} \tag{5}$$

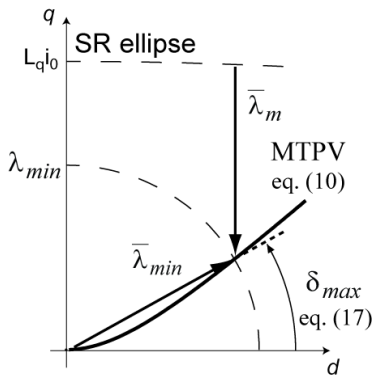

Figure 4. Example of determination of λ_m for a given SR motor with $\xi_{MTPV} = 5$, a given maximum speed (λ_{min}) and $k_{UCG} = 1$, that means the PM flux must be equal to the flux at maximum speed. δ_{max} is 27.4° according to (17) and $L_q i_0 = 1.45\ \lambda_{min}$.

For describing the maximum torque per voltage operation (that is practically equal to the maximum torque per flux operation, MTPF), it is convenient to express (5) in terms of the flux vector only, in amplitude and phase (6):

$$\bar{\lambda}_{dq} = \lambda \cdot \begin{bmatrix} \cos\delta \\ \sin\delta \end{bmatrix} \tag{6}$$

where the flux phase angle δ has been defined in Fig. 1. By substituting (2) and (6) into (5), the expression (7) is found.

$$T = \tfrac{3}{2}\, p \cdot \frac{1}{L_q} \left(\lambda^2 \cdot \frac{\xi - 1}{\xi} \cdot \frac{\sin 2\delta}{2} + \lambda \cdot \lambda_m \cdot \cos\delta \right) \tag{7}$$

The MTPV or MTPF trajectory in (λ , δ) coordinates can then be expressed by setting to zero the partial derivative of (7) with respect to δ. After some manipulation, (8) is found:

$$\left.\frac{\partial T}{\partial \delta}\right|_{\lambda = const} = 0 \Rightarrow 2 \cdot \sin^2\delta + \alpha \cdot \sin\delta - 1 = 0 \tag{8}$$

where the factor α has been introduced for simplifying the notation:

$$\alpha = \frac{\lambda_m}{\lambda} \cdot \frac{\xi}{\xi - 1} \tag{9}$$

The derivative of the term (ξ - 1) / ξ in (7) has been neglected in (8) for simplicity. Its impact in terms of accuracy is negligible, in particular for motors with high saliency. Moreover, the accuracy of the model relies on the choice of the proper ξ value, that is not known with precision until the motor is not designed and tested. The ξ value to be adopted in (9) will be indicated as ξ_{MTPV} in the following. The solution of (8) describes the MTPV flux trajectory in the *dq* flux plane (10).

$$\sin\delta_{MTPV} = \tfrac{1}{4} \cdot \left(-\alpha + \sqrt{\alpha^2 + 8} \right) \tag{10}$$

The example MTPV trajectory reported in Fig. 4 has been calculated according to (10).

F. Simplified expression of the CPSR (r)

As said in subsection II.B, we will consider the CPSR as the speed range between the rated flux (MTPA) situation at rated drive current i_0 and the crossing of the MTPV zone still at i_0, that is the maximum speed condition of our design. The definition (11) follows:

$$r = \frac{n_{max}}{n_{base}} \cong \frac{\lambda_{rated}}{\lambda_{min}} \tag{11}$$

The resistive drops have been neglected and λ_{rated} is the rated flux defined in Fig. 2. The rated flux is related through (12) to its *d*-axis component $\lambda_{rated,d}$, that is also equal to the *d*-axis flux component of the basic SR machine $\lambda_{r,rated,d}$.

$$\lambda_{rated,d} = \lambda_{r,rated,d} = \lambda_{rated} \cos\delta_{rated} \tag{12}$$

From Fig. 2 the *q*-component of the rated SR flux can be

written as $\lambda_{r,rated,q} = L_q\, i_{0,q} = L_q\, i_0\, sin\, \gamma_{rated}$. Then, multiplying and dividing (11) by $\lambda_{r,rated,d} / \lambda_{r,rated,q}$ the expression (13) is obtained.

$$r = \frac{\lambda_{rated}}{\lambda_{min}} = \frac{\lambda_{r,rated,d}}{\lambda_{r,rated,q}} \cdot \frac{\lambda_{rated}}{\lambda_{r,rated,d}} \cdot \frac{L_q\, i_0 \cdot sin\, \gamma_{rated}}{\lambda_{min}} \quad (13)$$

The SR flux component ratio in (13), can be developed as:

$$\frac{\lambda_{r,rated,d}}{\lambda_{r,rated,q}} = \frac{L_d}{L_q} \cdot \frac{i_{0,d}}{i_{0,q}} = \frac{\xi_{MTPA}}{tan\, \gamma_{rated}} \quad (14)$$

The MTPA saliency value ξ_{MTPA} is used in (14). The substitution of (12) and (14) into (13) gives (15).

$$r \cong \xi_{MTPA} \cdot \frac{cos\, \gamma_{rated}}{cos\, \delta_{rated}} \cdot \frac{L_q\, i_0}{\lambda_{min}} \quad (15)$$

In Fig. 4 the SR flux ellipse is well approximated by the horizontal line $\lambda_{r,q} = L_q\, i_0$. The relationship (16) then follows.

$$\lambda_m \cong L_q\, i_0 - \lambda_{min} \cdot sin\, \delta_{max} \quad (16)$$

Because of the design assumptions made in subsection II.C, the angle δ_{max} evidenced in the Fig. 4 is the maximum phase angle of the IPM motor flux in all operating conditions, and occurs at maximum speed, rated i_0 current. Its expression is obtained by substituting $\lambda = \lambda_{min}$ in (9) and (10).

$$sin\, \delta_{max} = \frac{1}{4} \cdot \left(-\alpha_{max} + \sqrt{\alpha_{max}^2 + 8} \right); \alpha_{max} = \frac{k_{UCG} \cdot \xi_{MTPV}}{\xi_{MTPV} - 1} \quad (17)$$

The angle δ_{max} shows a close relation with k_{UCG} through the α_{max} factor (17). The procedure for the design of λ_m is summarized by the two formulas (16) and (17), that must be applied iteratively until the obtained IPM motor fulfills the high speed specifications, i.e. a vector diagram like that of Fig. 4 is obtained. Anyway, the $\sin\delta_{max}$ value is typically lower than 0.5.

Back to the CPSR factor *r*, the term $L_q\, i_0$ in (15) is modified according to (16) and the expression (18) is finally found.

$$r = \xi_{MTPA} \frac{cos\, \gamma_{rated}}{cos\, \delta_{rated}} \cdot \left(k_{UCG} + sin\, \delta_{max} \right) \quad (18)$$

This is the relationship between the approximate CPSR and the UCG voltage factor (4). The angle γ_{rated} is defined in Fig. 2 and represents the current phase angle at low speed, according to the MTPA condition. The term ξ_{MTPA} represents the saliency of the motor at low speed and rated drive current. The angle δ_{rated} is typically low for a PMASR machine, since the flux orientation is not too far from the *d*-axis, as said.

In practical designs the rated flux λ_{rated} is limited by stator and rotor core saturation and the γ_{rated} current angle depends on many factors (e.g. motor size and current load) but it is usually $\gamma_{rated} > 45°$. Further indications about how to evaluate the saliency values ξ_{MTPA} , ξ_{MTPV} are given in section IV.

According to (18) it can be then concluded that:

- *the CPSR is strictly related to the UCG overvoltage (k_{UCG}): the CPSR can be increased to the detriment of a large UCG voltage;*
- *a high saliency is always welcome, giving a more favorable CPSR to k_{UCG} ratio.*

III. Relationship between UCG voltage, CPSR and drive current

Once the PMASR motor has been designed for a given drive current i_0 and a given maximum speed and CPSR, a certain UCG voltage follows. It has been demonstrated that the UCG voltage and the CPSR at rated drive current are related by (18). The CPSR is now evaluated again at reduced current amplitude, for finding out *which is the minimum current level i_1 that still guarantees a flat power curve up to the maximum speed*.

As the rated drive current i_0 is higher than the characteristic motor current, the reduction of the current amplitude will initially lead to a power profile that is even flatter, as the characteristic value is approached, as discussed in Section I. This can be seen by inspecting the curves with current values > i_{ch}. in Fig. 3b. Instead, as the current amplitude is under i_{ch} and is further reduced, the power profile tends progressively to curl, until the curve drops at rather limited speed values for very low current values (e.g. 0.35 i_{ch} in Fig. 3b). In conclusion: given the CPSR at rated drive current i_0, what is the current level $i_1 < i_0$ that still guarantees a flat curve up to the same ω_{max} obtained by i_0? The lower such current value is, the lower will be the sensitivity of the CPSR to current amplitude variations.

A straightforward approach for determining i_1 is proposed in Fig. 5: the current i_1 is defined as the one that reproduces at maximum speed a flux vector (of amplitude λ_{min}) that is mirrored with respect to the one obtained with i_0 (that is $\angle\bar{\lambda}_{min} = +\delta_{max}$ with i_0 and $\angle\bar{\lambda}_{min} = -\delta_{max}$ with i_1). This definition guarantees a good power factor at maximum speed and a power curve that is still flat, despite of the current that is lower than the characteristic one.

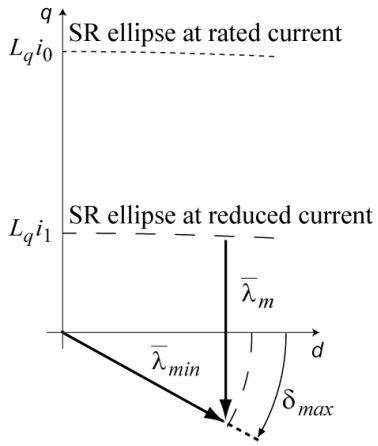

Figure 5. Determination of the reduced current i_1 according to the proposed criterion.

The relationship (19) follows.

$$L_q i_1 = \lambda_m - \lambda_{min} \cdot \sin \delta_{max} \quad (19)$$

By manipulating (16) and (19) the current ratio (20) is found.

$$\frac{i_1}{i_0} = \frac{\lambda_m - \lambda_{min} \cdot \sin \delta_{max}}{\lambda_m + \lambda_{min} \cdot \sin \delta_{max}} = \frac{k_{UCG} - \sin \delta_{max}}{k_{UCG} + \sin \delta_{max}} \quad (20)$$

As said, $\sin\delta_{max}$ is typically < 0.5, thus the current range (20) mainly depends on k_{UCG}. *With a high UCG overvoltage (e.g. k_{UCG} > 2) the current range from (20) results quite narrow and the drive is stiff from this point of view, while for low UCG overvoltage values the current interval is definitely larger. This once more confirms that a large CPSR can be conveniently pursued by means of a high saliency, for keeping k_{UCG} as low as possible (18) and have more flexibility towards current variations (20).* This approximated approach makes it easy to express the current interval i_1/i_0 analytically. Nevertheless, in most of PMASR motors current values lower than i_1 might still lead to quite flat power curves, thus the ratio (20) can be considered as a safe estimate. More accurate approaches are of course possible but they would require complicated models and would not change the general conclusions of this analysis. Dealing with PM flux variations due to temperature effects, the λ_m value considered in the design (16) and in the definition of k_{UCG} (4) was the one at operating temperature (hot conditions). Dealing with the actual UCG voltage, some margin must be safely introduced, since the worst case scenario of inverter fault occurs when the motor is cold. The PM flux realistically varies by 15% for a temperature variation of 120°C.

IV. Experimental Results

A. Motors under test

The approximated equations (18) and (20) are validated through measurements on two very different PMASR motor drives, whose specifications are reported in the Appendix.

- Motor 1, nameplate ratings are 470 W @ 3200 rpm, 18000 rpm maximum speed, designed for washing machines, shown in Figs. 6-7.
- Motor 2, nameplate ratings are 1 MW @ 250 rpm, 1350 rpm maximum speed, designed for a railway roller test bench, shown in Figs. 11-12.

B. Validation approach

To validate the proposed formulas (18) and (20) by means of already designed motors *it is necessary to turn upside down the approach that has been followed so far*. In sections II and III, the PM flux (λ_m) has been designed with reference to a specified maximum speed (i.e. at given λ_{min}) and it resulted in an UCG overvoltage factor (k_{UCG}). The reversed approach adopted here with given machines is:

- decide first a k_{UCG} factor to be tested.
- then verify equations (18), (20) according to the experimental identification of the machine.

Having an existing motor means that the PM flux (λ_m) is already determined and cannot be changed. Then, for any k_{UCG} a corresponding λ_{min} follows, according to (4). Given the rated motor voltage, this means that the maximum speed n_{max} is also determined by the choice of k_{UCG}, according to (3). Independently of what are the actual current and maximum speed the motor under test has been designed for, in this validation exercise the "rated" drive current i_0 will be also determined according to the chosen k_{UCG} and calculated, on the basis of the motor experimental data, as the current whose flux weakening trajectory encounters the MTPV curve exactly at λ_{min} , thus reproducing the vector diagram of Fig. 4. Once i_0 is so determined, the rated flux vector λ_{rated} is calculated as the flux amplitude corresponding to i_0 , on the experimental MTPA curve. The base speed and then the CPSR also follow, from V_{rated} and λ_{rated} (3). The reduced current i_1 is calculated as the current amplitude that produces the same λ_{min} with mirrored flux phase angle $-\delta_{max}$, as in Fig. 5. Finally, the so obtained CPSR and i_0/i_1, evaluated from the experimental data, are compared with the results from (18) and (20).

C. Results with Motor 1

The steady-state magnetic behavior of the motor has been identified in the current range i_d = 0 to 5 A pk, i_q = 0 to 5 A pk, following the measurement procedure described in [13].

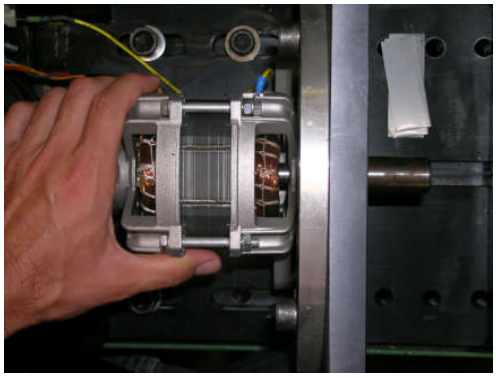

Figure 6. Motor 1.

Figure 7. Rotor lamination of Motor 1.The PM bonded (ferrite) material is injected in the hollow flux barriers

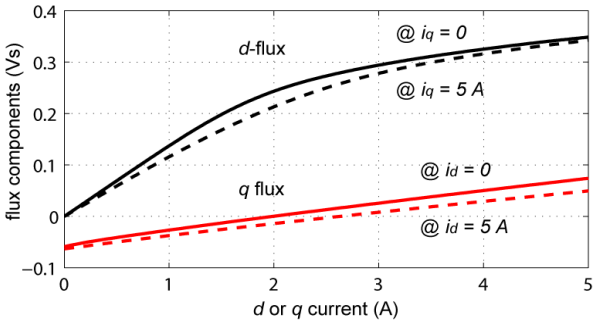

Figure 8. Magnetic curves of Motor 1, measured at steady state.The intermediate flux values are obtained by interpolation, following the approach described in [13].

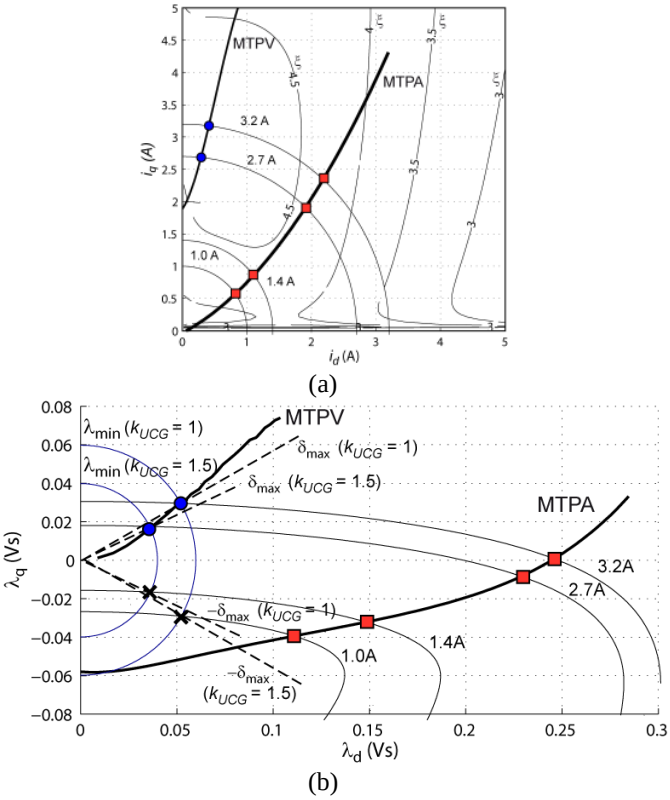

Figure 9. MTPA, MTPV, constant current and constant flux curves of the motor for a washing machine, based on the experimental data. a) *dq* current plane; b) *dq* flux plane.

The resulting flux versus current experimental curves are reported in Fig. 8. Based on the experimental data, the MTPA, MTPV, constant current and constant flux trajectories can be plotted, both in the (i_d , i_q) and (λ_d , λ_q) planes, as in Fig. 9. Two different k_{UCG} factors (1.0 and 1.5) and their corresponding λ_{min} values are considered for the evaluation of r and i_0/i_1. The PM flux is 0.06 Vs (Figs. 8, 9, i_d = i_q = 0), then λ_{min} is 0.06 Vs in the former case and 0.04 Vs in the latter. With the rated voltage specified in the Appendix, the respective maximum speeds are 12000 rpm (k_{UCG} = 1) and 18000 rpm (k_{UCG} = 1.5). The i_0 current is calculated in the flux frame of Fig. 9b by determining which of the constant-current-amplitude curve (pseudo ellipse) intersects the MTPV trajectory in correspondence of the λ_{min} circle. The angles δ_{max} follow in both cases. Finally, the current i_1 is individuated from the intersection of its "ellipse" with the λ_{min} circle at -δ_{max}. In the examples of Fig. 9b, k_{UCG} = 1 leads to i_1 = 1.0 A, i_0 = 3.2 A and k_{UCG} = 1.5 leads to i_1 = 1.4 A, i_0 = 2.7 A. The power profiles at all current amplitudes are calculated on the basis of the experimental model and reported in Fig. 10. The base and maximum speed points have been evidenced in Fig. 10 by means of square and circle tags, respectively, and the CPSR can be evaluated in the two cases. The same squares and circles have been reported also in Fig. 9 for better clarity. The power profiles of Fig. 10 point out that the lower the CPSR is the larger the i_0/i_1 ratio is.

Dealing with the application of (18) and (20) for evaluating r and i_0/i_1 respectively, the motor saliency and the γ_{rated}, δ_{rated} angles are estimated again from the motor experimental curves. The saliency values ξ_{MTPA} and ξ_{MTPV} might be roughly evaluated from the flux curves of Fig. 8. For better clarity, the experimental data have been manipulated to obtain the saliency map in the (i_d, i_q) plane reported in Fig. 9a: the saliency has been calculated from the chord inductances. Along the MTPA curve, for both 2.7 A and 3.2 A, the current phase angles and the saliency values are close to each other and shown in Table I. δ_{rated} is practically zero (Fig. 9b, squares at 2.7 and 3.2 A).

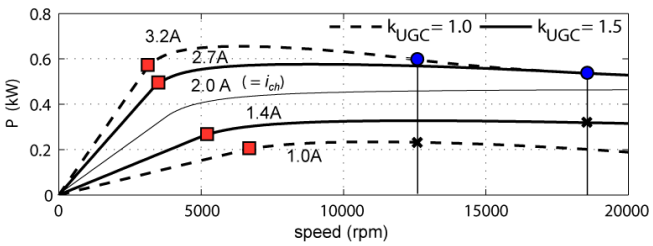

Figure 10. Power profiles of Motor 1, based on the experimental data.

TABLE I. MOTOR 1 (470W): COMPARISON BETWEEN THE SIMPLIFIED EQUATIONS (18. 20) AND THE EXPERIMENTAL DATA

		k_{UCG}	1.0	1.5
Experimental data	Fig.9b	i_0 (A)	3.2	2.7
		i_1 (A)	1.0	1.4
		i_1/i_0	**0.31**	**0.52**
	Fig. 10	γ_{rated}	47	45
		n_{base} (rpm)	3000	3200
		n_{max} (rpm)	12500	18500
		r	**4.2**	**5.8**
	Fig. 9a	ξ_{MTPA}	4.3	4.4
		ξ_{MTPV}	4.6	4.6
Proposed model	Eq. 17	sin δ_{max}	0.45	0.37
	Eq. 18	**r**	**4.3**	**5.8**
	Eq. 20	**i_1/i_0**	**0.37**	**0.60**

Along the MTPV curve ξ_{MTPV} = 4.6 will be used in equation (17) for determining δ_{max} both at 2.7 A and 3.2 A. Anyway, the sensitivity of δ_{max} to ξ is very low (17), at least for the considered anisotropy values. The results coming from (18) and (20) are compared in Table I to the values coming from experiments, showing a fairly good correspondence.

D. Results with Motor 2

The steady-state magnetic model of the motor, identified in the current range i_d = 0 to 1130 A pk, i_q = 0 to 1700 A pk , is reported in Fig. 13. The corresponding MTPA, MTPV and other significant trajectories are plotted in the (i_d , i_q) and (λ_d , λ_q) planes in Fig. 14. The r and i_0/i_1 formulas are verified here with reference to k_{UCG} = 1.55. This value has been chosen instead of 1.50 because this one would have required the knowledge of the experimental magnetic model over a current range larger than the available one. The PM flux is 2.0 Vs (Figs. 13, 14b, $i_d = i_q = 0$), then λ_{min} is 1.29 Vs. With the rated voltage specified in the Appendix, the maximum speed is 1270 rpm. The application of the procedure described in subsection IV.C leads to i_1 = 860 A, i_0 = 1500 A , from the experimental curves. The corresponding power profiles are the ones in Fig. 15. The application of the formulas follows the evaluation of γ_{rated} = 58°, ξ_{MTPA} = 6, ξ_{MTPV} = 8 (all from Fig. 14a), δ_{rated} = 0° (Fig. 14b).

Figure 11. Motor 2.

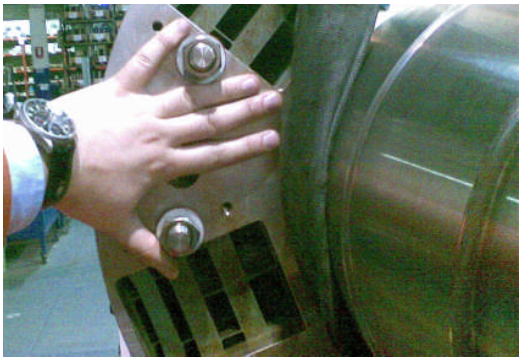

Figure 12. Motor 2: detail of the hollows housing the inset PMs, seen from the inspection windows of one of the flanges of the rotor stack.

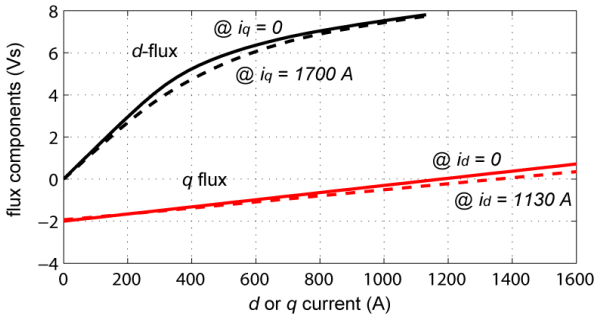

Figure 13. Magnetic curves of Motor 2, measured at steady state.

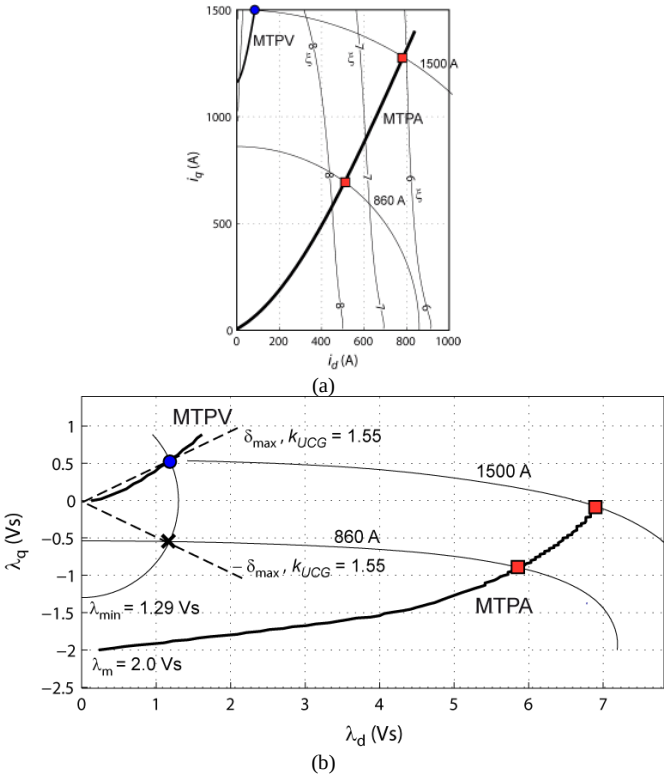

Figure 14. Motor 2: MTPA, MTPV, constant current and constant flux curves of the motor for a railway roller test bench, based on the experimental data. a) *dq* current plane; b) *dq* flux plane.

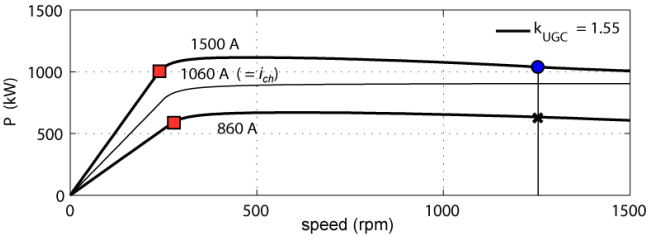

Figure 15. Motor 2. power profiles of the motor for a railway roller test bench, based on the experimental data.

The results of (18) and (20) are compared with the experimental values in Table II. As for Motor 1, the estimate of the current ratio i_0/i_1 is in the direction of safety (estimated

i_1 greater than the experimental one). As for the CPSR, the r estimate from (18) is here 10% larger than real: this may be attributed to the large sensitivity to the motor saliency, that is very high in this case. Anyway, it looks still a fairly good result, for an approximated formula.

TABLE II
MOTOR 2 (1 MW): COMPARISON BETWEEN THE SIMPLIFIED EQUATIONS (18. 20) AND THE EXPERIMENTAL DATA

		$\boldsymbol{k_{UCG}}$	**1.55**
Experimental data	Fig. 15	i_0 (A)	1500
		i_1 (A)	860
		$\boldsymbol{i_1/i_0}$	**0.57**
	Fig. 14	γ_{rated}	60°
		n_{base} (rpm)	240
		n_{max} (rpm)	1270
		$\boldsymbol{r}$	**5.3**
	Fig. 13	ξ_{MTPA}	6
		ξ_{MTPV}	8
Proposed model	Eq. 12	$\sin \delta_{max}$	0.39
	Eq. 18	$\boldsymbol{r}$	**5.8**
	Eq. 20	$\boldsymbol{i_1/i_0}$	**0.60**

V. CONCLUSIONS

Two simple formulas have been introduced, giving better evidence to the effects of some design choices, when a CPSR is required from an interior permanent magnet motor drive. These formulas, starting from the expected value of the rotor saliency, allow the preliminary calculation of the obtainable CPSR and current span of the related IPM drive, with no need of the complete design procedure. This gives evidence to some important conclusions about the expected drive performance. A first general conclusion is drawn that maximization of the motor anisotropy is welcome, for having a large CPSR with a low UCG voltage. Second, it has been shown that large current spans are compatible with large CPSRs and again this is possible with large rotor saliency values. As a practical consequence, general purpose drives of the PM-assisted synchronous reluctance type can be designed and built, provided that the rotor saliency is properly maximized.

APPENDIX

The ratings of the two motors under test are reported in Tables III and IV. The inductance values are not reported in the tables because they can be derived by inspection of the magnetic curves of Figs. 8 and 13 for motors 1 and 2 respectively. The power curves can be derived from Fig. 10 (Motor 1) and Fig. 15 (Motor 2), apart from iron and mechanical losses.

TABLE III - NAMEPLATE RATINGS OF MOTOR 1

Torque	1.4 Nm
Line to line voltage	270 V pk
Phase current	2.8 A pk
Base speed	3200 rpm
Maximum speed	18000 rpm
Back-emf at base speed (line to line)	70 V pk
Characteristic current	2.0 A pk
Pole pairs	2
Stator diameter, stack length	55.2 - 35 mm

TABLE IV – NAMEPLATE RATINGS OF MOTOR 2

Torque	38500 Nm
Line to line voltage	877 V pk
Phase current	1470 A pk
Base speed	250 rpm
Maximum speed	1350 rpm
Back-emf at base speed (line to line)	272 V pk
Characteristic current	1160 A pk
Pole pairs	3
Stator diameter, stack length	980 - 1500 mm

REFERENCES

[1] T. M. Jahns, G. B. Kliman, and T. W. Neumann, “Interior permanent magnet synchronous motors for adjustable-speed drives”, IEEE Trans. Ind. Appl., vol. IA-22, pp. 738-747, July/Aug. 1986.

[2] R. Schiferl,T.A. Lipo, “Power capability of Salient pole P.M. synchronous motors in variable speed drive”, Conf. Record. of IEEE-IAS annual meeting 1988, pp: 23-31.

[3] Zhu, Z.Q.; Howe, D.; , "Electrical Machines and Drives for Electric, Hybrid, and Fuel Cell Vehicles," *Proceedings of the IEEE* , vol.95, no.4, pp.746-765, April 2007

[4] Harson, A.; Mellor, P.H.; Howe, D.; , "Design considerations for induction machines for electric vehicle drives," *Electrical Machines and Drives, 1995. Seventh International Conference on (Conf. Publ. No. 412)* , vol., no., pp.16-20, 11-13 Sep 1995

[5] W. Soong and T. J. E. Miller, “Field weakening performance of brushless synchronousAC motor drives,” Proc. IEE—Elect. Power Appl., vol. 141, no. 6, pp. 331–340, Nov. 1994.

[6] EL-Refaie, A.M.; Jahns, T.M., "Optimal flux weakening in surface PM machines using fractional-slot concentrated windings," *Industry Applications, IEEE Transactions on* , vol.41, no.3, pp. 790-800, May-June 2005

[7] T. M. Jahns and V. Caliskan, “Uncontrolled generator operation of interior PM synchronous machines following high speed inverter shutdown,” *IEEE Trans. Ind. Appl.*, vol. 35, pp. 1347–1357, Nov./Dec. 1999.

[8] A. Fratta, A. Vagati, F. Villata, “Design criteria of an IPM machine suitable for field-weakening operation”, International Conference on Electrical Machines, ICEM90, Boston 1990, U.S.A., pp: 1059-1065.

[9] Morimoto, S.; Sanada, M.; Takeda, Y., "Performance of PM-assisted synchronous reluctance motor for high-efficiency and wide constant-power operation," *Industry Applications, IEEE Transactions on* , vol.37, no.5, pp.1234-1240, Sep/Oct 2001

[10] N. Bianchi, S. Bolognani, A. Consoli, T.M. Jahns, R.D. Lorenz, E.C. Lovelace, S. Morimoto, A. Vagati, “Design, analysis, and control of interior PM synchronous machines”, in Proc. IEEE IAS Tutorial Course Notes, IAS Annu. Meeting, Seattle, WA: CLEUP, Oct. 3, 2004.

[11] Vagati, A.; Pellegrino, G.; Guglielmi, P.; , "Comparison between SPM and IPM motor drives for EV application," *Electrical Machines*

(ICEM), 2010 XIX International Conference on , vol., no., pp.1-6, 6-8 Sept. 2010

[12] P. Guglielmi, E. Armando, G.M. Pellegrino, A.Vagati, "Optimal design of IPM-PMASR motors for wide constant power speed range," Proc. of PCIM 2007, PCIM Europe, Nurnberg 2007- Germany.

Gianmario Pellegrino (M'06) received the M.Sc. and Ph.D. degrees in electrical engineering from Politecnico di Torino, Turin, Italy, in 1998 and 2002, respectively.

He has been a Guest Researcher at Aalborg University, Denmark, in 2002. Since 2002 he has been with Politecnico di Torino, first as a Research Associate and then as an Assistant Professor, since 2007. He has been a visiting fellow at Nottingham University, UK, in 2010/2011. He is involved in research projects within the industry. He has more than 50 technical papers and one patent. His research areas are the electrical machines and drives, namely, the motor design and the digital control.

Dr. Pellegrino is an Associate Editor for the IEEE Transactions on Industry Applications. He is the corecipient of the IEEE-IAS EMC 3rd Paper Paper Award for ECCE 2009, the IEEE-IAS IDC 3rd Paper Paper Award for ECCE 2010 and the ICEM 2010 Best Paper Award.

Alfredo Vagati (M'88–SM'92–F'98) received the Laurea degree in Electrical Engineering from Politecnico di Torino, Turin, Italy, in 1970.

After a few years working in industry with Olivetti, he joined Politecnico di Torino in 1975, as Assistant Professor. In 1990, he became Professor of Electrical Machines and Drives at the University of Cagliari, Italy. In 1991, he rejoined Politecnico di Torino in the same capacity. From 1995 to 2003 He was the Head of the Electrical Engineering Department of Politecnico di Torino and member of the Academic Senate from 2005 to 2009. His scientific activity, in the field of electrical machines and drives, has been focused on high-performance ac drives. He has been involved in several industrial projects in the field of ac drives, as both a designer and a scientific reference. His most relevant activity has concerned the design and control of a family of newly developed, high-performance synchronous reluctance (SyR) an permanent magnet assisted synchronous reluctance (PMASR) motors. He has led several national and European research projects in the field of design and control of synchronous-machine-based drives for many different applications, including home appliances and the automotive world. He has authored or coauthored more than 100 technical papers.

Prof. Vagati is a Fellow Member of the IEEE Society. He is also a member of the Advisory Board of PCIM, International Conference and Exhibition.

Paolo Guglielmi (M'07) received the M.Sc. degree in electronic engineering and the Ph.D. degree in electrical engineering from the Politecnico di Torino, Turin, Italy, in 1996 and 2001, respectively.

In 1997, he joined the Department of Electrical Engineering, Politecnico di Torino, where he became a Researcher in 2002. He has authored several papers published in technical journals and conference proceedings. His fields of interest include power electronics, high performance drives, and computer-aided design of electrical machines.

[13] A.Vagati, M.Pastorelli, F.Scapino, and G.Franceschini. "Impact of cross saturation in synchronous reluctance motors of the transverse-laminated type". *IEEE Trans. Ind. Appl.*, vol. 36 (4), pp. 1039–1046, 2000.